



Conditional Knockout of GLT-1 in Neurons Leads to Alterations in Aspartate Homeostasis and Synaptic Mitochondrial Metabolism in Striatum and Hippocampus

Laura F. McNair¹ · Jens V. Andersen¹ · Jakob D. Nissen¹ · Yan Sun² · Kathryn D. Fischer² · Nathaniel W. Hodgson² · Muzi Du³ · Chiye J. Aoki^{3,4} · Helle S. Waagepetersen¹ · Paul A. Rosenberg^{2,5} · Blanca I. Aldana¹

Received: 3 October 2019 / Revised: 6 February 2020 / Accepted: 25 February 2020 / Published online: 6 March 2020
© Springer Science+Business Media, LLC, part of Springer Nature 2020

Abstract

Expression of the glutamate transporter GLT-1 in neurons has been shown to be important for synaptic mitochondrial function in the cerebral cortex. Here we determined whether neuronal GLT-1 plays a similar role in the hippocampus and striatum, using conditional GLT-1 knockout mice in which GLT-1 was inactivated in neurons by expression of synapsin-Cre (synGLT-1 KO). Ex vivo ¹³C-labelling using [1,2-¹³C]acetate, representing astrocytic metabolism, yielded increased [4,5-¹³C]glutamate levels, suggesting increased astrocyte-neuron glutamine transfer, in the striatum but not in the hippocampus of the synGLT-1 KO. Moreover, aspartate concentrations were reduced – 38% compared to controls in the hippocampus and the striatum of the synGLT-1 KO. Mitochondria isolated from the hippocampus of synGLT-1 KO mice exhibited a lower oxygen consumption rate in the presence of oligomycin A, indicative of a decreased proton leak across the mitochondrial membrane, whereas the ATP production rate was unchanged. Electron microscopy revealed reduced mitochondrial inter-cristae distance within excitatory synaptic terminals in the hippocampus and striatum of the synGLT-1 KO. Finally, dilution of ¹³C-labelling originating from [U-¹³C]glucose, caused by metabolism of unlabelled glutamate, was reduced in hippocampal synGLT-1 KO synaptosomes, suggesting that neuronal GLT-1 provides glutamate for synaptic tricarboxylic acid cycle metabolism. Collectively, these data demonstrate an important role of neuronal expression of GLT-1 in synaptic mitochondrial metabolism in the forebrain.

Keywords Glutamate · Glutamine · Brain energy metabolism · TCA cycle · Forebrain

Introduction

Rapid clearance of released neurotransmitter glutamate is essential for efficient neuronal signalling. The high-affinity glutamate transporter GLT-1 (EAAT2; SLC1A2) mediates cellular uptake of glutamate and is abundantly expressed in astrocytes, but is also found in pre-synaptic axon terminals of glutamatergic neurons [1, 2]. Neuronal GLT-1 is expressed in several brain regions including the cerebral cortex [3], hippocampus [4, 5] and striatum [6], whereas it is absent in other regions including the brain stem and cerebellum [7]. However, the importance of neuronal GLT-1 across brain regions is just starting to be unravelled [8]. Prolonged synaptic exposure to glutamate, as a result of impaired clearance, can cause excitotoxicity, and has been linked to several neurodegenerative diseases [9–13]. Interestingly, brain regions exhibit differential susceptibility to

Special issue: In Honor of Professor Michael Robinson.

Laura F. McNair and Jens V. Andersen contributed equally to this work as co-first authors and Paul A. Rosenberg and Blanca I. Aldana contributed equally to this work as co-senior authors.

Electronic supplementary material The online version of this article (<https://doi.org/10.1007/s11064-020-03000-7>) contains supplementary material, which is available to authorized users.

✉ Blanca I. Aldana
blanca.aldana@sund.ku.dk

Extended author information available on the last page of the article

neurodegenerative diseases, as for example, the striatum is severely affected during Huntington's disease, whereas Alzheimer's disease primarily affects the cerebral cortex and hippocampus [14, 15]. Interestingly, deletion of neuronal GLT-1 has been found to produce a Huntington's disease-like pattern of transcriptional dysregulation, suggesting that specific impairments of neuronal glutamate uptake or downstream metabolic or signalling pathways impacted by expression of neuronal GLT-1 might be involved in disease development [16].

Apart from being a neurotransmitter, glutamate can also be oxidatively metabolized in the tricarboxylic acid (TCA) cycle [17, 18]. This is important in both astrocytes and neurons and serves as a link between neurotransmission and cellular energy metabolism [19–21]. Brain energy metabolism is heterogeneous throughout different brain regions [22], as are the level of metabolic enzyme expression [23–25] and mitochondrial function [26, 27]. We have recently shown that specific knock-out of neuronal GLT-1 in mice (synGLT-1 KO mice) leads to significant alterations in metabolism, and mitochondrial morphology and dynamics in the cerebral cortex [28]. To extend these findings, we investigated the potential metabolic effects of neuronal GLT-1 knock out in two other brain regions, namely the hippocampus and striatum. We applied ex vivo metabolic mapping using [1-¹³C]glucose and [1,2-¹³C]acetate, to map neuronal and astrocytic metabolism, respectively. Furthermore, we investigated hippocampal mitochondrial energetics and synaptosomal glucose metabolism in the synGLT-1 KO mice. Finally, we used electron microscopy to assess the effect of synGLT-1 KO on the prevalence of mitochondrial profiles within glutamatergic axon terminals in both the striatum and hippocampus.

Materials and Methods

Materials

The stable isotopes [1-¹³C]glucose, [1,2-¹³C]acetate and [U-¹³C]glucose (all 99% purity) were purchased from Cambridge Isotope Laboratories (Tewksbury, MA, USA). All other chemicals were of the purest grade available from regular commercial sources.

Mice

Male conditional GLT-1 knockout mice (*Slc1a2^{tm1.1Pros}*, MGI: 5,752,263), in which the GLT-1 gene was inactivated in neurons by expression of synapsin-Cre as previously described (synGLT-1 KO; GLT-1^{Δ/Δ}; syn-Cre+) [29], and littermate controls with normal GLT-1 function (GLT-1^{fllox/fllox}; syn-Cre-) were obtained from the founder colony

at Boston Children's Hospital. Additional control animals included wild-type mice (GLT-1^{w/w}; syn-Cre-) and littermates expressing the synapsin-Cre (GLT-1^{w/w}; syn-Cre+). Throughout this manuscript, 'Controls' refer to the GLT-1^{fllox/fllox}; syn-Cre- littermates, unless specified otherwise.

Mice were housed in humidity- and temperature-controlled facilities, on a 12/12 h light/dark cycle (7:00 A.M. to 7:00 P.M. light), with free access to standard chow and water. Animal experiments were conducted at Boston Children's Hospital (USA) and University of Copenhagen (Denmark). A first set of experiments included ex vivo assessment of neural metabolism including 45- to 54-weeks-old mice, and follow-up studies to confirm and extend findings in the first set of experiments were conducted on two further cohorts of mice (8–40 weeks-old).

Ex Vivo Metabolic Mapping by Nuclear Magnetic Resonance (NMR) Spectroscopy

The ex vivo metabolic mapping using NMR spectroscopy was performed as described previously [28]. Briefly, seven synGLT-1 KO and seven control mice (45–54 weeks of age) were injected intraperitoneally with 0.3 M [1-¹³C]glucose (543 mg/kg) in combination with 0.6 M [1,2-¹³C]acetate (504 mg/kg) and euthanized 15 min after injection by focused microbeam irradiation to the head (Gering Applied Engineering, Inc. instrument, Canada). Mice were decapitated and brain regions of interest were dissected and sonicated in methanol. Amino acids of the brain homogenate were extracted by water-methanol-chloroform extraction (5:2:2, V:V:V). Samples were lyophilized and dissolved in deuterium oxide containing 8 mM [2,2,3,3-d(4)-3-(trimethylsilyl)propionic acid sodium salt and 0.2% (V/V) ethylene glycol as internal standards. Spectra were obtained using either a 600 MHz Bruker Avance III or Avance III HD (Bruker BioSpin GmbH, Reinstetten, Germany) equipped with 1.7 mm inverse TXI-probe and a 5 mm dual DCH-probe (both cryogenically cooled), respectively. All samples were prepared in 1.7 mm O.D. NMR-tubes (30–50 μL), which were inserted into 2.5 mm tubes for analysis with the 5 mm probe head. ¹H-NMR spectra were acquired using a pulse angle of 90°, 12 kHz spectral width with 64 k data points, acquisition time of 2.66 s, relaxation delay of 10 s and 128 scans. Proton decoupled ¹³C-NMR spectra were obtained using 30° pulse angle and 30 kHz spectral width with 98 k data points employing an acquisition time of 1.65 s and a relaxation delay of 0.5 s. The number of scans were adjusted to get an adequate signal to noise ratio (defined as > 3 for the [4,5-¹³C]glutamate signal, one of the weaker signals expected with the ¹³C-substrates injected in the current study) which was approximately 14,000 scans (8 h) using the DCH-probe on a cerebral sample. TopSpin 3.2

software (Bruker BioSpin GmbH, Reinstetten, Germany) was used for acquisition, processing and analysis.

Mitochondrial Oxygen Consumption Rate and ATP Synthesis Rate

Hippocampal mitochondria were isolated from three synGLT-1 KO and three control mice (8–20 weeks of age), as described previously [30]. All procedures were performed on ice or at 4 °C. Briefly, animals were euthanized by cervical dislocation and the brain submerged in ice cold artificial cerebrospinal fluid containing in mM: NaCl 128, NaHCO₃ 25, D-glucose 10, KCl 3, CaCl₂ 2, MgSO₄ 1.2, KH₂PO₄ 0.4, pH = 7.4. The hippocampi were dissected and transferred to an isolation buffer (MSHE) containing in mM: mannitol 210, sucrose 70, HEPES 5, EGTA 1 and 0.5% BSA (fatty acid free), pH = 7.2, and homogenised using a Teflon douncer, 750 revolutions/min for 7–8 strokes. Homogenate was centrifuged (500 g × 5 min) and the pellet discarded. The supernatant was centrifuged (14,000 g × 10 min) and the pellet re-suspended in 12% Percoll MSHE solution. The 12% Percoll MSHE suspension was layered on top of 21% Percoll MSHE solution and further centrifuged (18,000 g × 15 min). The supernatant was discarded and the mitochondrial fraction was rinsed with two subsequent centrifugations (18,000 g × 5 min and 14,000 g × 5 min) by suspending the mitochondria in MSHE and discarding the supernatant after each centrifugation. The final mitochondrial pellet was re-suspended in MSHE and the amount of protein was determined by the Bradford method.

The oxygen consumption rate (OCR, pmol/min) of the isolated hippocampal mitochondria was assessed at 37 °C using a Seahorse XFe96 analyzer (Seahorse Biosciences, MA, USA) [30]. Mitochondria were suspended in assay (MAS) buffer containing in mM: mannitol 220, sucrose 70, KH₂PO₄ 10, MgCl₂ 5, HEPES 2 and 0.2% bovine serum albumin (BSA) (fatty acid free), pH = 7.2. 4 µg of protein was added to each well and the plate was centrifuged (2,000 g × 20 min) at 4 °C. The mitochondria were provided 37 °C MAS buffer containing 10 mM pyruvate with 2 mM malate or 10 mM glutamate with 10 mM malate (all final concentrations) and analysed immediately. Four compounds were injected during the experiment in the following order: ADP (4 mM), oligomycin A (2.5 µg/mL), carbonyl cyanide-p-trifluoromethoxyphenylhydrazone (FCCP, 8 µM) and antimycin A (8 µM), all final concentrations. Data was extracted using the Wave software (Seahorse Biosciences). Relative OCR levels were calculated by setting the OCR at the third baseline measurement to 100%.

The rate of ATP synthesis (nmol ATP/(min × mg protein)) of the isolated hippocampal mitochondria was assessed with an ATP/luciferin based assay as previously described [30]. Briefly, the isolated mitochondria were diluted in buffer,

containing in mM: sucrose 250, K₂HPO₄ 15, MgSO₄ 2, EDTA 0.5 and 0.5% BSA (fatty acid free), pH = 7.2 and 2.5 µg of protein was added to each well. The wells contained either pyruvate or glutamate, and P1, P5-diadenosine pentaphosphate in final concentrations of 5 mM and 10 µM, respectively. During the measurement period, three injections were performed: first, a luciferin-luciferase cocktail was injected to establish the background luminescence. Subsequently, 2 mM ADP in combination with 2.5 mM malate (final concentrations) was injected and lastly 250 µM ATP was added as an internal standard.

Synaptosomal Glutamate Uptake and Metabolism

Synaptosomes were isolated by two different methods: *purified* synaptosomes were used for incubations with [U-¹³C] glucose whereas *crude* synaptosomes were used for investigation of synaptosomal glutamate uptake. Purified hippocampal synaptosomes were isolated from five synGLT-1 KO and four control mice (8–10 weeks of age) as previously described [19] and crude hippocampal and striatal synaptosomes were isolated from three or six synGLT-1 KO and three or six control mice, respectively, (8–10 weeks of age) as previously described [29].

Synaptosomal glutamate uptake was determined by sodium-dependent transport of L-[³H]glutamate as previously described [29]. The isolated crude synaptosomes were exposed to 10 µM L-glutamate [including 5 nM L-[³H]glutamate (Perkin Elmer)] for 30 s at 37 °C. Uptake activity was terminated by adding ice-cold choline buffer. The samples were filtered through Whatman GF/C filter paper and radioactivity on the filters was measured by liquid scintillation counting. The radioactivity taken up by the synaptosomes in the absence of sodium was subtracted from that taken up in the presence of sodium to determine the sodium-dependent component of transport. Glutamate uptake values were determined by normalizing the radioactivity count by protein concentration of the crude synaptosomes isolated from each brain region.

Synaptosomal glutamate metabolism was assessed in purified hippocampal synaptosomes (0.3 mg protein/condition) by incubation for 45 min at 37 °C (DMEM without fetal calf serum, pH 7.4; DMEM) containing 2.5 mM [U-¹³C]glucose and 0.1 mM unlabelled glutamate [28]. Incubations were terminated by centrifugation (1000 g × 2 min at 4 °C) and the synaptosomes were washed once with phosphate-buffered saline and extracted with 70% ice-cold ethanol. Synaptosome extracts and incubation media were lyophilized before gas chromatography-mass spectrometry (GC-MS) and high performance liquid chromatography (HPLC), to determine ¹³C enrichment in TCA cycle intermediates and amino acids, and amino acid amounts, respectively [31]. Lactate was assayed using a lactate assay kit

(R-Biopharm AG, Darmstadt, Germany) and protein content was determined using the Pierce bicinchoninic acid protein assay.

Electron Microscopy Analysis

The CA1 field of dorsal hippocampus and dorsal striatum of three synGLT-1 KO and three controls (8–10 weeks of age) were employed for ultra-structural analysis. Only hippocampal tissue was immunolabelled for GLT-1 using HRP-DAB-osmium as described previously [29]. Briefly, electron microscopic images were captured at a magnification of 40,000X. Imaging was conducted by sweeping across surface-most portions of (immunolabelled) vibratome sections, until the number of profiles of asymmetric (presumably excitatory) synaptic junctions reached 100 per animal in striatum and 50 per animal in hippocampus.

Within the neuropil area occupying the targeted number of excitatory synaptic junctions, the following was assessed: (1) average number of presynaptic mitochondrial profiles, per every group of 10 excitatory synaptic profiles encountered (“pre-synaptic mitochondria, per 10 synapses”); (2) average number of mitochondrial profiles within peri-synaptic astrocytic profiles, per every group of 10 synapses (“peri-synaptic astrocytic mitochondria, per 10 synapses”); and (3) the occurrence of tripartite synapses, per every group of 10 synapses. For the hippocampus, only, we also assessed (4) average number of astrocytic mitochondrial profiles encountered per unit area.

In the previous study [28], we had shown that mitochondrial cristae density, which reflects mitochondria’s efficiency of ATP production [32], is increased for cortical tissue of synGLT-1 KO, relative to controls. In order to determine whether such an ultrastructural change also occurs in hippocampus and striatum, mitochondrial cristae density within excitatory presynaptic axonal terminals was assessed by measuring the distance between two or more adjacent cristae at the point of junction with the inner mitochondrial membrane, as described in [32]. Electron microscopic images were captured at a magnification (40,000×) that allowed generation of sufficiently high-resolution images for determining the density of mitochondrial profiles. The same images were further enlarged by 200% to measure distances between clearly visible cristae using ImageJ version 1.51 k (NIH, Bethesda, MD, USA). A supplementary Online Resource 1 and caption has been provided to demonstrate the inter-cristae measuring procedure.

The number of mitochondria analysed per animal was 35 for the hippocampus, reflecting all mitochondria encountered within an area spanning 50 excitatory synapses that were encountered through systematic sweeping along surface-most portions of vibratome sections and overlapping with the area sampled to attain the four values listed

above, plus additional mitochondria to reach a sample size of 35. The number of mitochondria analysed per animal was approximately 30 for dorsal striatum, contained within an area in which 100 excitatory synapses were encountered through systematic sweeping of the neuropil. These values were reported in graph as “Distance between neighbouring cristae”. All values were pooled across tissue derived from the same genotype, for assessing whether the values differed significantly across the genotypes. The tissue used for these analyses had been assessed previously, confirming efficient and specific GLT-1 knockout from neurons in hippocampus [29].

Statistics

Student’s *t*-test was used when comparing groups, except for the EM data for which non-parametric tests were applied as appropriate, and comparisons between multiple groups concerning HPLC-determined metabolite concentrations for which a 2-way ANOVA analysis was employed. To reduce the possibility of Type I error, we regarded $p < 0.05$ (indicated by an asterisk in the figures) as statistically significant. To correct for multiple comparisons using the Student’s *t*-test, we used the Benjamini–Hochberg procedure with a critical value for false discovery of 0.10 [33]. All data are represented as mean \pm standard error of the mean (SEM). All statistical analyses were conducted using Prism (GraphPad).

Results

GLT-1 has been shown to be expressed in axon terminals in the hippocampus and striatum by immunohistochemistry in addition to the cerebral cortex [3–6]. Multiple experiments were conducted on synGLT-1 KO (GLT-1 $^{\Delta/\Delta}$; syn-Cre+) and littermate control mice (GLT-1 $^{flox/flox}$; syn-Cre-) to assess if the essential role of neuronal GLT-1 in synaptic glutamate homeostasis and mitochondrial function extends from cerebral cortex [28] to these two other brain regions. In particular, we conducted: assessment of total metabolite concentrations in extracts of whole brain regions, ex vivo metabolic ^{13}C -mapping to elucidate neuronal and astrocyte energy metabolism; electron microscopy (EM) to assess mitochondrial density within peri-synaptic astrocyte processes and presynaptic terminals of excitatory neurons, and determine mitochondrial cristae density; measurements of oxygen consumption and ATP production in isolated mitochondria to investigate electron transport chain functionality, and assessments of glycolytic activity, glutamate uptake, and metabolic ^{13}C -mapping experiments in synaptosome preparations to separate out changes specific to synapses. Certain experiments were conducted only for one of the two brain regions as will be detailed below.

Synaptosomal Glutamate Uptake

First we measured uptake of L-[³H]glutamate in crude synaptosomes derived from the hippocampus and striatum. We found that glutamate uptake was significantly reduced in synGLT-1 KO mice compared to controls in synaptosomes prepared from hippocampus (84% reduction; $p = 0.038$, $n = 3$) and striatum (53% reduction; $p = 0.002$, $n = 6$; Fig. 1). These data provide additional evidence for the expression of GLT-1 in axon terminals of these brain regions [5, 7, 28, 29], the efficacy of the synapsin-Cre driven KO of GLT-1, and the competence of neuronal GLT-1 in these regions to mediate glutamate transport.

Ex Vivo Metabolic Mapping in Hippocampus and Striatum

Total Metabolite Concentrations

Initial studies of total metabolite concentrations were assayed by ¹H-NMR in a cohort of mice which had been subjected to ex vivo metabolic ¹³C-mapping using injectable [1-¹³C]glucose/[1,2-¹³C]acetate. Hippocampal (49 ± 13 mg, $n = 14$) and striatal (37 ± 15 mg, $n = 14$) tissue was successfully collected from seven synGLT-1 KO and seven control mice. Interestingly, this cohort displayed no significant changes in aspartate levels in the synGLT-1 KO compared to controls when assayed by ¹H-NMR (hippocampus; $p = 0.105$, striatum: $p = 0.885$, both $n = 7$; Table 1). In light of our previous study in the cerebral cortex revealing highly

reduced aspartate concentrations (–44–57%) in the synGLT-1 KO animals in comparison to controls by ¹H-NMR and HPLC, a second cohort of animals was used to ascertain the effects of the neuronal GLT-1 KO on aspartate concentrations in hippocampus and striatum by HPLC. Here we found that synGLT-1 KO mice in comparison to controls exhibited significantly reduced aspartate levels in the hippocampus (38%, $p = 0.005$, $n = 11–12$; Fig. 2a) as well as in the striatum (38%, $p = 0.02$, $n = 5–7$; Fig. 2b) of the synGLT-1 KO in comparison to controls.

The expression of Cre-recombinase (Cre) is known to result in a range of untargeted effects in eukaryotic cells [34–38]. Hence, in this set of experiments additional controls were included to ascertain that findings could not be attributed the Cre-expression itself. In particular, we assayed total concentrations of aspartate, glutamate and GABA using HPLC in wild-type mice (GLT-1^{w/w}; syn-Cre–) and littermates expressing synapsin-Cre (GLT-1^{w/w}; syn-Cre+) in both hippocampus and striatum, and found no significant differences between these groups ($p > 0.05$, $n = 11–13$; Fig. 2), confirming that the Cre-expression in itself does not affect amino acid homeostasis.

The concentration of additional metabolites measured by ¹H-NMR in the first cohort of animals (alanine, creatine, phosphocreatine, total creatine, fumarate, GABA, glutamate, glutamine, lactate, m-Inositol, N-acetyl aspartate, succinate and tyrosine) were not significantly altered in the synGLT-1 KO animals compared to controls ($p > 0.05$, $n = 7$; Table 1). One exception, however, was hippocampal myo-inositol levels, which were significantly higher (–19%) in the hippocampus of synGLT-1 KO compared to controls ($p = 0.025$, $n = 7$). The lack of effects on metabolite pools, other than aspartate and myo-inositol, from the synGLT-1 KO, suggests overall maintained neural health. Of note, N-acetyl aspartate levels which are an indicator of neuronal health [39, 40] were unaffected, indicating absence of neurodegeneration in these mice. The unchanged concentrations of GABA and glutamate in the hippocampus and striatum of synGLT-1 KO animals were also tested by HPLC in the second cohort of animals. GABA concentrations were similar in hippocampal tissue from control (3.1 ± 0.3 $\mu\text{mol/g}$) and synGLT-1 KO animals (2.6 ± 0.2 $\mu\text{mol/g}$), as were concentrations of glutamate (control: 16.8 ± 0.8 $\mu\text{mol/g}$, synGLT-1 KO: 15.8 ± 0.9 $\mu\text{mol/g}$; both $p > 0.05$, $n = 11–12$). The same held true for striatal concentrations of GABA (control: 5.4 ± 0.2 $\mu\text{mol/g}$, synGLT-1 KO: 6.2 ± 0.3 $\mu\text{mol/g}$) and glutamate (control: 8.4 ± 0.9 $\mu\text{mol/g}$, synGLT-1 KO: 10.3 ± 0.7 $\mu\text{mol/g}$; both $p > 0.05$, $n = 5$).

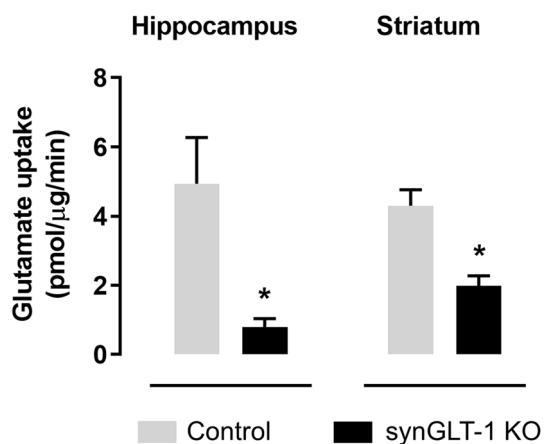


Fig. 1 Glutamate uptake is reduced in crude synaptosomes prepared from hippocampus and striatum of synGLT-1 KO mice. Synaptosomes were generated from brain tissue of mice in which the GLT-1 gene was knocked out in neurons by expression of synapsin-Cre (synGLT-1 KO; black bars) and controls (grey bars). Synaptic glutamate uptake was determined using L-[³H]glutamate. Results are presented as mean \pm SEM; hippocampus: $n = 3$, striatum: $n = 6$; * $p < 0.05$, Student's *t*-test

Metabolism of [1-¹³C]Glucose

It has been shown that [1-¹³C]glucose-derived metabolites primarily reflects neuronal energy metabolism and

Table 1 Total metabolite concentrations ($\mu\text{mol/g}$ tissue) in extracts of whole hippocampus and striatum determined by $^1\text{H-NMR}$

Metabolite	Hippocampus			Striatum		
	Control	synGLT-1 KO	<i>p</i>	Control	synGLT-1 KO	<i>p</i>
Alanine	0.46 ± 0.09	0.47 ± 0.09	0.904	0.19 ± 0.02	0.27 ± 0.06	0.191
Aspartate ^a	1.62 ± 0.34	0.97 ± 0.03	0.105	0.80 ± 0.05	0.78 ± 0.14	0.885
Creatine	4.47 ± 0.30	4.41 ± 0.30	0.872	3.11 ± 0.40	3.10 ± 0.36	0.991
P-Creatine	1.17 ± 0.35	1.76 ± 0.34	0.252	1.23 ± 0.19	1.23 ± 0.26	0.991
Total creatine	6.17 ± 0.25	5.64 ± 0.26	0.175	4.34 ± 0.51	4.33 ± 0.45	0.989
Fumerate	0.06 ± 0.01	0.06 ± 0.01	0.905	0.03 ± 0.00	0.03 ± 0.00	0.552
GABA	1.29 ± 0.15	1.48 ± 0.17	0.426	1.34 ± 0.16	1.51 ± 0.20	0.514
Glutamate ^a	7.17 ± 0.33	7.42 ± 0.10	0.507	5.21 ± 0.58	5.31 ± 0.63	0.905
Glutamine	4.74 ± 0.31	5.16 ± 0.50	0.492	3.06 ± 0.44	2.35 ± 0.45	0.280
Lactate ^a	2.09 ± 0.52	1.43 ± 0.31	0.316	0.89 ± 0.11	0.91 ± 0.17	0.923
Myo-inositol	4.26 ± 0.23	5.08 ± 0.23	0.025	3.01 ± 0.37	3.30 ± 0.36	0.586
N-Acetyl aspartate	4.83 ± 0.31	5.22 ± 0.36	0.425	3.88 ± 0.45	3.67 ± 0.45	0.745
Succinate	N.D.			0.31 ± 0.04	0.28 ± 0.03	0.557
Tyrosine	0.11 ± 0.01	0.12 ± 0.01	0.486	0.09 ± 0.01	0.09 ± 0.01	0.774

The table summarizes concentrations of total (labelled and unlabelled) metabolites in extracts of hippocampus and striatum tissue obtained by $^1\text{H-NMR}$ spectroscopy. Tissue was collected from synGLT-1 KO and control mice following injection with $[1-^{13}\text{C}]\text{glucose}/[1,2-^{13}\text{C}]\text{acetate}$. Results are presented as mean ± SEM; $n = 7$. Total creatine = phosphocreatine + creatine; NAA, *N*-acetyl aspartate.

^aUsing ROUT’s method, outliers were detected and excluded from synGLT-1 KO hippocampal data (aspartate 2.4, lactate 10.3, glutamate 10.0 $\mu\text{mol/g}$ tissue) and striatal data (lactate 6.4 $\mu\text{mol/g}$ tissue), hence, $n = 6$ for these data set. N.D. designates ‘not determined’ due to peak intensities in $^1\text{H-NMR}$ spectra being too low for reliable integration

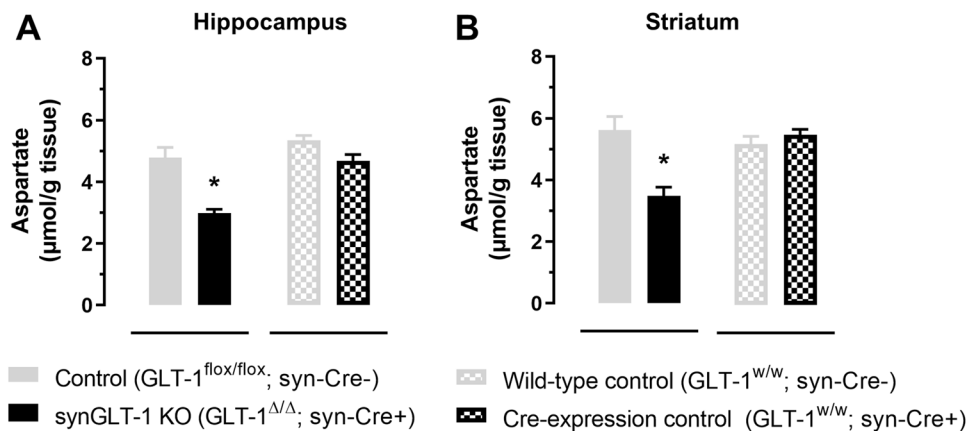


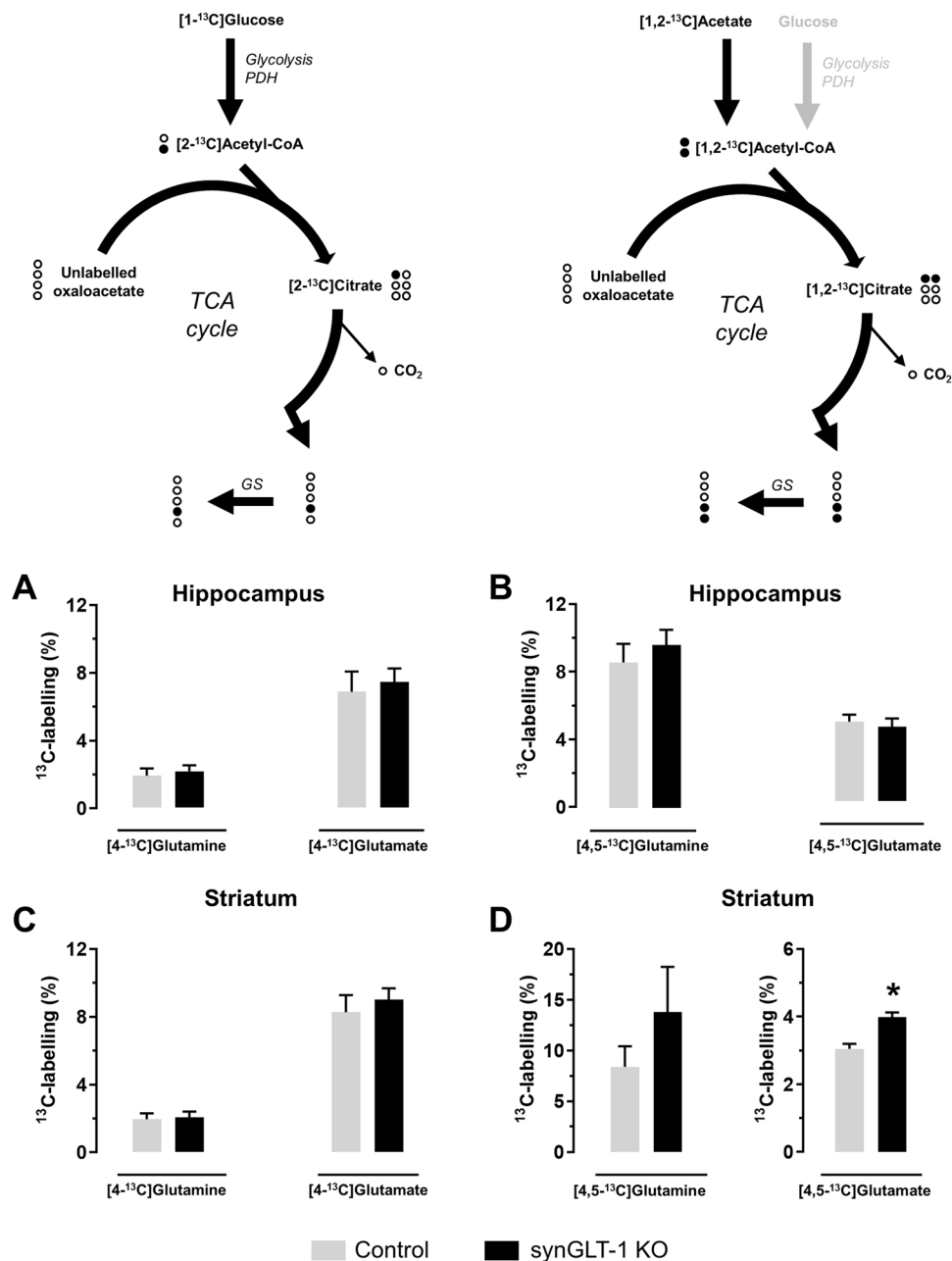
Fig. 2 Reduced aspartate concentrations in forebrain regions of synGLT-1 KO. Total metabolite concentrations were assayed by HPLC in extracts of hippocampus (a) and striatum (b) from synGLT-1 KO mice (GLT-1^{Δ/Δ}; syn-Cre+, black bars) and controls (GLT-1^{flx/flx}; syn-Cre-, grey bars) as well as wild-type mice (GLT-1^{w/w}; syn-Cre-,

grey checkered bars) and littermates expressing the synapsin-Cre (GLT-1^{w/w}; syn-Cre+, black checkered bars). Results are presented as mean ± SEM; hippocampus: $n = 11-13$, striatum: $n = 5-7$; * $p < 0.05$, 2-way ANOVA

the formation of glutamine from glutamate synthesized in neurons [41–43]. Hippocampus and striatum exhibited no significant differences between synGLT-1 KO and control mice in the ^{13}C -labelling (%) of glutamate or glutamine derived from the first turn of the TCA cycle metabolism of $[2-^{13}\text{C}]\text{acetyl-CoA}$ generated from $[1-^{13}\text{C}]\text{glucose}$, that

is, $[4-^{13}\text{C}]\text{glutamate}$ (hippocampus: $p = 0.694$, striatum: $p = 0.600$; $n = 7$) and $[4-^{13}\text{C}]\text{glutamine}$ (hippocampus: $p = 0.652$, striatum: $p = 0.837$; $n = 7$; Fig. 3a & c). First turn of the TCA cycle metabolism of $[2-^{13}\text{C}]\text{acetyl-CoA}$ derived from $[1-^{13}\text{C}]\text{glucose}$ also leads to formation of $[2-^{13}\text{C}]$ and $[3-^{13}\text{C}]\text{oxaloacetate}$, which upon second turn of the TCA

Fig. 3 Ex vivo metabolic mapping experiments suggest elevated astrocyte-neuron glutamine transfer in striatum but not hippocampus, and detect no TCA cycle metabolism changes in either striatum or hippocampus of synGLT-1 KO mice. Percentage ^{13}C -labelling in glutamate and glutamine following intraperitoneal injection with $[1-^{13}\text{C}]$ glucose (**a** hippocampus and **c** striatum) and $[1,2-^{13}\text{C}]$ acetate (**b** hippocampus and **d** striatum) assesses in vivo neuronal and astrocytic metabolism, respectively. Black and white circles in the top illustration represent ^{13}C and ^{12}C , respectively. 15 min post-injection mice were euthanized by microwave fixation of the brain, which was then dissected and individual regions (hippocampus and striatum) assayed for the percentage ^{13}C -labelling in glutamine and glutamate originating from metabolism of the ^{13}C -labelled substrates using ^1H -NMR and ^{13}C -NMR. Results are presented as mean \pm SEM; $n=7$; * $p < 0.05$, Student's t -test



cycle gives rise to glutamate and glutamine likewise labelled at these positions. Hence, the ratio between the products of first and second turn TCA cycle metabolism provides an alternative estimate of the TCA cycle activity [44]. The TCA cycling ratios calculated for hippocampus and striatum as $[3-^{13}\text{C}]\text{glutamate}/[4-^{13}\text{C}]\text{glutamate}$ were not significantly different in brain tissue obtained from the GLT-1 KO compared to control ($p > 0.05$, $n=6-7$; data not shown).

Comparison of TCA cycling ratios for hippocampus, striatum (current study) and cerebral cortex (previous study, [28]) from control animals revealed no significant differences (1-way ANOVA, $p > 0.05$, $n=6-7$; data not shown). These observations suggest that neuronal TCA cycling

activity, which can be measured by this ex vivo technique, is similar in these three brain regions.

Metabolism of $[1,2-^{13}\text{C}]\text{Acetate}$

$[1,2-^{13}\text{C}]\text{Acetate}$ is preferentially metabolized by astrocytes and the metabolite ^{13}C -labelling primarily reflects astrocyte metabolism [45]. The ^{13}C -enrichment (%) in glutamate and glutamine derived from $[1,2-^{13}\text{C}]\text{acetate}$ following first turn of the TCA cycle was not significantly different in the synGLT-1 KO compared to controls in the hippocampus (Fig. 3b). In contrast, whereas the percentage $[4,5-^{13}\text{C}]\text{glutamate}$ in hippocampus was unaffected by the KO ($p=0.661$),

striatum from synGLT-1 KO mice exhibited a 31% larger enrichment of [4,5-¹³C]glutamate compared to controls ($p=0.001$, $n=7$; Fig. 3d), derived from astrocyte metabolism of [1,2-¹³C]acetate.

Ultrastructural Characterisation of Mitochondria in Astrocytes and Neurons

We recently showed that in the cerebral cortex genetic deletion of neuronal GLT-1 causes increased prevalence of mitochondrial profiles in neurons and peri-synaptic astrocyte processes, paralleled by reduced distance between intra mitochondrial cristae [28]. Glutamatergic synaptic terminals are especially dense in the hippocampus and in the striatum because of the presence of prominent intrahippocampal and corticostriate excitatory pathways. Therefore, we were interested in whether lack of neuronal GLT-1 expression would affect the prevalence of mitochondrial profiles and the inter-cristae distance within mitochondrial profiles of axon terminals in these regions as well. For this purpose, we examined hippocampal and striatal tissue at the ultra-structural level using electron microscopy (EM).

Ultrastructural Analysis of Hippocampus

EM analysis of the hippocampus was performed from stratum radiatum of the dorsal hippocampal CA1 field. Representative EM images of hippocampal tissue from control and synGLT-1 KO mice are shown in Fig. 4a–c. Immunolabelled axon terminals were identified as excitatory, based on the thickness of post-synaptic densities along the intracellular surface of the dendritic shaft and spine plasma membrane facing the synaptic cleft (arrowheads in Fig. 4a–c). For this cohort of animals, we have previously reported that the occurrence of axon terminals forming excitatory synapses and exhibiting GLT-1 immunoreactivity was significantly lower in hippocampus of synGLT-1 KO, compared to control ($2 \pm 2\%$ for synGLT-1 KO versus $16 \pm 4\%$ for controls, $p < 0.01$; [29]). The same animal cohort samples were used to complete the additional microstructural analyses presented below. The occurrence of excitatory synapses in the hippocampus associated with astrocytic processes, i.e. formation of tripartite synapses, was not significantly different in synGLT-1 KO tissue (9.5 ± 0.2 per 10 synapses) in comparison with control [9.6 ± 0.2 per 10 synapses, $p=0.8$, $t=0.2467$, $df=26.10$; Welch's t -test ($n=15$ for each genotype, 5 groups of 10 synapses analysed per animal, pooled across three animals per genotype)].

The occurrence of mitochondria within axon terminals forming excitatory synapses was significantly higher in the hippocampus of synGLT-1 KO mice (4.3 ± 0.5) compared to controls [1.9 ± 0.3 mitochondria per 10 synapses; $p=0.0003$, $t=4.209$, $df=25.28$; Welch's t -test, ($n=15$ for

each genotype, 5 groups of 10 synapses per animal, pooled across three animals per genotype); Fig. 4d]. Similarly, the occurrence of mitochondria within hippocampal astrocytic processes associated with excitatory synapses was significantly higher in synGLT-1 KO (1.1 ± 0.3) compared to controls [0.3 ± 0.1 per 10 synapses; $p=0.008$, $U=52$; Mann–Whitney test ($n=15$ for each genotype, 5 groups of 10 synapses per animal, pooled across three animals per genotype); Fig. 4e]. In line with this observation, the occurrence of mitochondria in astrocytes both with and without contact with excitatory synapses was significantly higher for synGLT-1 KO (0.58 ± 0.09 per unit area of $10.5 \mu\text{m}^2$) compared to control tissue [0.20 ± 0.06 per unit area of $10.5 \mu\text{m}^2$; $p=0.003$, $U=1605$; Mann–Whitney test ($n=86$ for synGLT-1 KO, $n=50$ for controls, encompassing the area occupied by 50 excitatory synapses per animal and pooled across three animals per genotype); Fig. 4f]. Finally, the inter-cristea distances within pre-synaptic mitochondria was found to be significantly decreased by the KO of GLT-1 in neurons [control: 59 ± 2 nm; synGLT-1 KO: 53 ± 2 nm; $p=0.005$, $U=5280$; Mann–Whitney test ($n=105$ for each genotype, 35 mitochondria per animal and pooled across three animals per genotype); Fig. 4g)].

Ultrastructural Analysis of Dorsal Striatum

EM analysis was also performed in dorsal striatum of the same animals. Representative EM images of striatal tissue from control and synGLT-1 KO mice are shown in Fig. 5a–c. As observed for the hippocampus, the occurrence of excitatory synapses in hippocampus associated with astrocytic processes, i.e. formation of tripartite synapses, was not significantly different in synGLT-1 KO tissue (7.8 ± 0.2 per 10 synapses) in comparison with control [8.1 ± 0.3 per 10 synapses, $p=0.5$, $t=0.6561$, $df=57.55$; Welch's t -test ($n=30$ for each genotype, 10 groups of 10 synapses analysed per animal, pooled across three animals per genotype)]. Notably, comparison across brain regions revealed that the occurrence of tripartite synapses (synGLT-1 KO and control data pooled) was significantly lower in dorsal striatum (8.0 ± 0.2 per 10 synapses) than in hippocampus [9.6 ± 0.2 per 10 synapses, $p < 0.0001$, $t=7.305$, $df=87.62$; Welch's t -test ($n=30$ for hippocampus, $n=60$ for striatum, 5 groups of 10 synapses analysed per animal for dorsal hippocampus and 10 groups of 10 synapses analysed per animal for dorsal striatum, pooled across six animals per brain region)].

Unlike the pattern observed for the hippocampus, the occurrence of mitochondrial profiles within axon terminals forming excitatory synapses in the striatum was not significantly different between the genotypes [3.1 ± 0.4 mitochondria per 10 synapses for synGLT-1 KO mice; 3.5 ± 0.4 for control; $p=0.4$, $t=0.8547$, $df=57.35$; Welch's t -test ($n=30$ for each genotype, 10 groups of 10 synapses pooled across

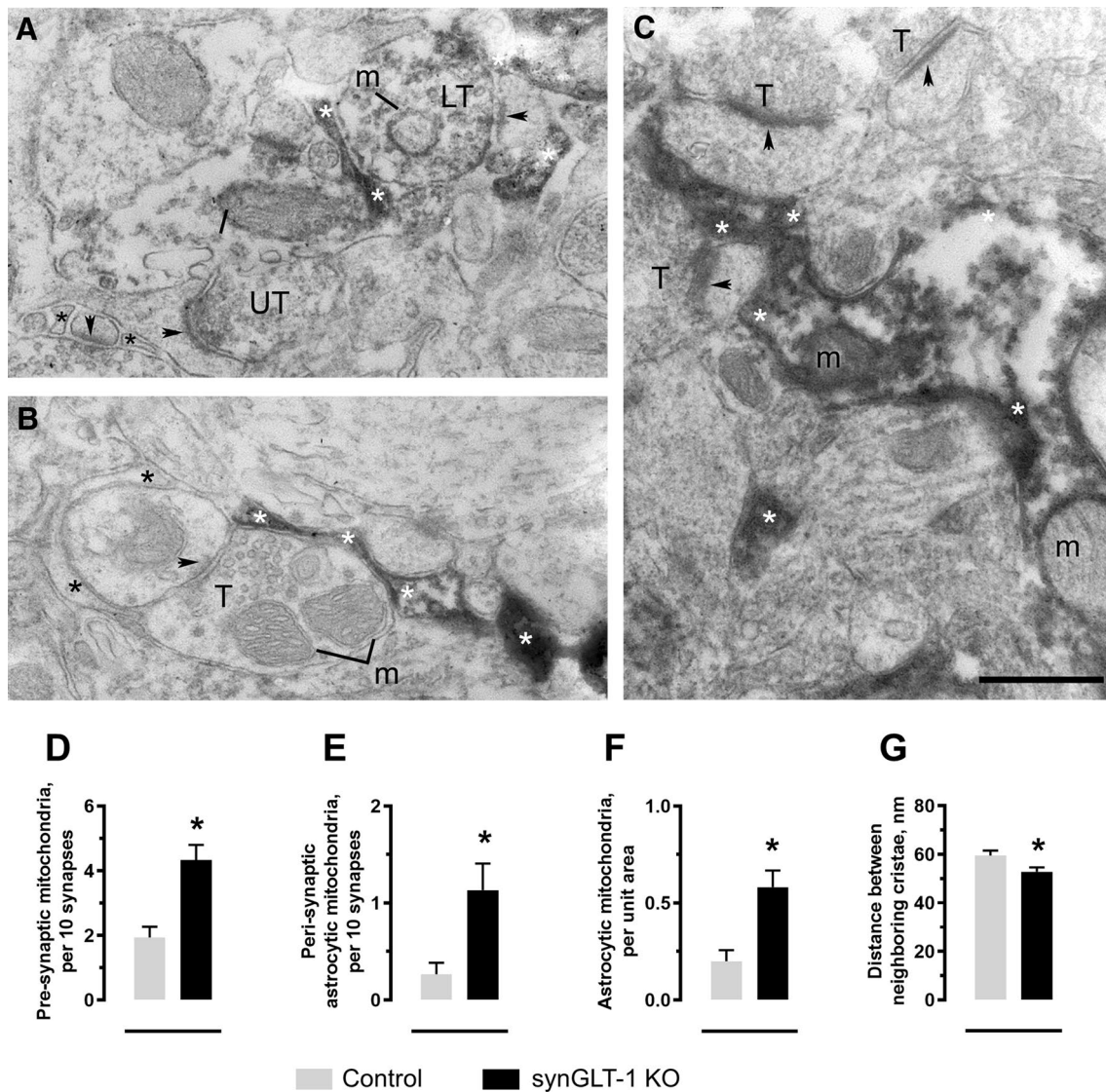


Fig. 4 Electron microscopy reveals increased occurrence of mitochondrial profiles within astrocytes and excitatory axon terminals of hippocampus in synGLT-1 KO mice. Representative electron microscopic images of a synaptic neuropil in hippocampal tissue from control mouse (**a**) and mice in which the GLT-1 gene was knocked out in neurons by expression of synapsin-Cre (synGLT-1 KO; **b**, **c**). Immunocytochemistry reveals GLT-1 immunoreactivity in some of the axon terminals forming excitatory synapses onto dendritic spines of control but rarely within the hippocampus of synGLT-1 KO mice. Samples were imaged from stratum radiatum of dorsal hippocampal CA1. T: axon terminal; LT: axon terminal immunolabelled for GLT-1. Arrowheads point to thick postsynaptic densities within dendritic spine; m: mitochondria. White asterisks indicate astrocytic processes with GLT-1 immunoreactivity of both control and synGLT-1 KO neuropil, indicated by the diffuse electron dense material distributed in the cytoplasm and along the plasma membrane that form irregular,

scalloped and triangular contours that tightly surround excitatory synapses. Note that some astrocytic profiles lack GLT-1 immunoreactivity (black asterisks in **a** and **b**). Control tissue shows GLT-1 immunoreactivity in axon terminals of some (LT, immunolabelled) but not all (UT, unlabelled). None of the axon terminals of the synGLT-1 KO animal in these micrographs exhibit GLT-1 immunoreactivity. Calibration bar: 500 nm. All three micrographs were taken at a magnification of 40,000 \times . Quantitative analyses reveals increased density of mitochondria in axon terminals forming excitatory axo-spinous synapses ($n=15$ for both genotypes; **d**), in peri-synaptic astrocytic processes ($n=15$ for both genotypes; **e**), and in all encountered astrocytic profiles ($n=50$ and 86 for controls and synGLT-1 KO, respectively; **f**). Inter-cristae distance for mitochondrial profiles in neuronal terminals were significantly reduced ($n=105$ for both genotypes; **g**). Results are presented as mean \pm SEM; * $p < 0.05$, non-parametric tests as specified in main text

three animals per genotype); Fig. 5d]. Similarly, the occurrence of mitochondria in peri-synaptic astrocytes was rare and not different for synGLT-1 KO (0.6 ± 0.2) compared to controls [0.7 ± 0.2 per 10 synapses; $p=0.60$, $U=418.5$;

Mann Whitney test ($n=30$ for each genotype, 10 groups of 10 synapses per animal, pooled across three animals per genotype); Fig. 5e]. A difference across genotypes was detected for the averaged inter-cristae distances within pre-synaptic

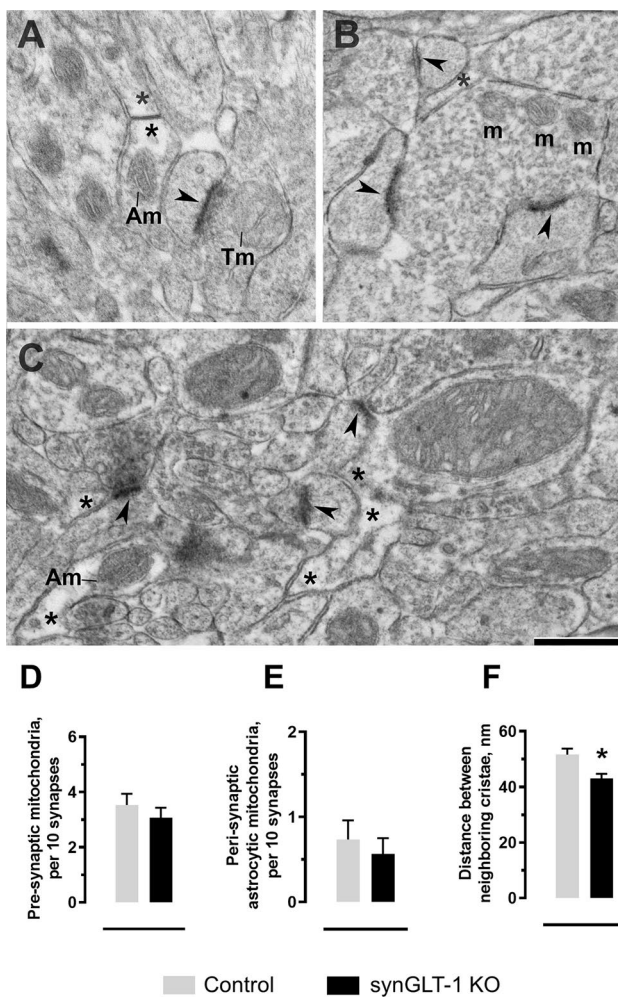


Fig. 5 Electron microscopic analysis of dorsal striatum reveals no change in the occurrence of mitochondrial profiles within astrocytes or excitatory axon terminals but reduced average inter-cristae distance for mitochondria within excitatory axon terminals. Representative electron microscopic images of the synaptic neuropil in dorsal striatum from control mouse (**a**) and synGLT-1 KO mice (**b** and **c**) are shown. These tissues did not undergo immunocytochemical labeling for GLT-1. Arrowheads point to thick postsynaptic densities of axo-spinous synapses, indicating that these synapses are excitatory. Asterisks point to the cytoplasm of astrocytic profiles, identified based on the scalloped and triangular contours that tightly surround presynaptic terminals and postsynaptic dendrites forming excitatory synapses. In **a**, two astrocytic processes have come together to form a gap junction (in between the two asterisks), which is another morphological feature characteristic of astrocytic processes. Am and Tm: mitochondrial profiles within astrocytic processes and axon terminals, respectively. Calibration bar: 500 nm. All micrographs were captured at a magnification of 40,000 \times . The occurrence of mitochondrial profiles within axon terminals of dorsal striatum forming excitatory axo-spinous synapses (**d**), within peri-synaptic astrocytic processes (**e**) and averaged inter-cristae distance for each mitochondrial profile encountered within a neuropil area spanning approximately 100 excitatory synapses per animal (**f**) were assessed from electron microscopic images such as these. Results are presented as mean \pm SEM. * $p < 0.05$, non-parametric tests as specified in main text

mitochondrial profiles [control: 52 ± 2 nm; synGLT-1 KO: 43 ± 2 nm; $p = 0.0008$, $U = 2814$, Mann–Whitney test ($n = 92$ and $n = 86$ mitochondria, pooled from control and synGLT-1 KO tissue of three animals, respectively, spanning an area occupied by 100 excitatory synapses per animal); Fig. 5f].

Oxygen Consumption and ATP Production in Mitochondria Isolated from Hippocampus

In order to elucidate if the altered mitochondrial morphology observed by EM of the synGLT-1 KO would be accompanied by an altered mitochondrial metabolism, oxygen consumption and ATP production was assessed in mitochondria isolated from the hippocampus. In mitochondria, glutamate may be converted to the TCA cycle intermediate α -ketoglutarate via transamination or glutamate dehydrogenase, and thereby improve the metabolic capacity of the mitochondria. Hence, experiments measuring ATP production and oxygen consumption in isolated mitochondria were designed to assess the effects of neuronal GLT-1 KO on electron transport chain functionality.

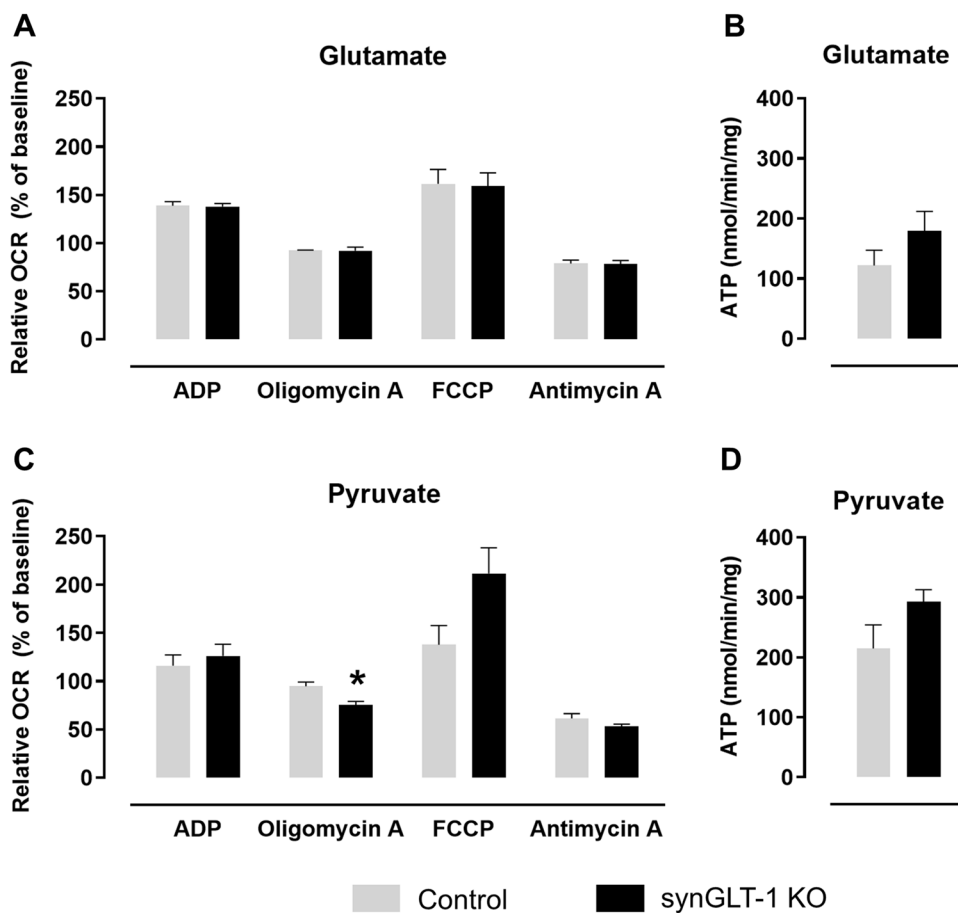
Respiration of isolated mitochondria from hippocampus of synGLT-1 KO and control mice was assessed in the presence of malate combined with either glutamate or pyruvate, respectively. No significant differences in the oxygen consumption were observed between synGLT-1 KO and control mitochondria for the malate-glutamate condition following addition of the four modulatory compounds: (1) ADP to stimulate coupled respiration generating ATP, (2) oligomycin A to inhibit the ATP synthase and test if the mitochondria are intact and coupled, (3) FCCP to induce proton leakage across the mitochondrial membrane leading to maximal uncoupled respiration, and (4) antimycin A to inhibit complex III of the electron transport chain ($p > 0.05$, $n = 3$; Fig. 6a). For the malate-pyruvate condition, mitochondrial uncoupling following addition of FCCP did not result in significantly altered oxygen consumption in synGLT-1 KO compared to control ($p = 0.089$, $n = 3$; Fig. 6c). However, a significant reduction in oxygen consumption was observed in synGLT-1 KO compared to control upon oligomycin A application ($p = 0.029$, $n = 3$, Fig. 6c). Finally, no changes in the ATP production rate in the synGLT-1 KO compared to controls was observed in the presence of either glutamate and pyruvate ($p = 0.23$ and 0.15 , respectively, $n = 3$, Fig. 6b & d).

Synaptosomal Glutamate Metabolism in Hippocampus

Total Metabolite Concentrations

In order to dissect out the effects of the neuronal GLT-1 KO specifically on synaptic metabolism, concentrations of

Fig. 6 Mitochondrial function is altered in the hippocampus of synGLT-1 KO mice. **a** Mitochondria were isolated from hippocampus of synGLT-1 KO mice (black bars) and littermate controls (grey bars). The oxygen consumption rate (OCR) was measured in mitochondria in media containing malate, and glutamate (**a**) or pyruvate (**c**), in the presence of (1) ADP to stimulate coupled respiration generating ATP, (2) oligomycin A to inhibit the ATP synthase, (3) FCCP to induce proton leakage across the mitochondrial membrane leading to maximal uncoupled respiration, and (4) antimycin A to inhibit complex III of the electron transport chain. ATP production was assayed in mitochondria in media containing malate, and glutamate (**b**) or pyruvate (**d**). Results are presented as mean \pm SEM; $n=3$; * $p<0.05$, Student's *t*-test



metabolites were determined in synaptosome preparations of hippocampus following incubation in medium containing 2.5 mM [U- 13 C]glucose and 0.1 mM unlabelled glutamate. In contrast to the ex vivo measurements, no significant differences between synGLT-1 KO and control were observed for total aspartate concentrations, which were assessed by HPLC ($p>0.05$, $n=4-5$). Likewise, no significant changes were observed for any other metabolites measured (glutamate, glutamine, serine, alanine, valine, isoleucine and leucine; $p>0.05$, $n=4-5$; Table 2).

TCA Cycle Metabolism

We have previously shown that synGLT-1 KO leads to decreased TCA cycle metabolism of glutamate in synaptosomes of the cerebral cortex [28]. 13 C-Labeling data from synaptosomes incubated in media containing [U- 13 C]glucose and unlabelled glutamate was employed to estimate the influx of unlabelled carbon from glutamate into the TCA cycle intermediate pool. More specifically, the unlabelled glutamate influx was assessed employing the ratio between percentage metabolite M + 2 and the sum of percentages for the remaining isotopologues (M + 1, M + 3 etc.; see [28] for further details). This ratio was

Table 2 Total amino acid concentrations (nmol/mg protein) in extracts of hippocampal synaptosomes determined by HPLC

Metabolite	Control	synGLT-1 KO	<i>p</i>
Aspartate	18.43 \pm 4.05	17.14 \pm 2.58	0.787
Glutamate	35.70 \pm 6.81	42.49 \pm 7.09	0.519
Serine	2.32 \pm 0.38	3.01 \pm 0.53	0.348
Glutamine	1.70 \pm 0.46	1.65 \pm 0.33	0.930
Alanine	1.92 \pm 0.16	1.80 \pm 0.21	0.670
GABA	3.95 \pm 0.80	4.69 \pm 0.74	0.524
Valine	2.09 \pm 0.37	2.14 \pm 0.38	0.916
Isoleucine	2.53 \pm 0.32	2.71 \pm 0.39	0.746
Leucine	2.49 \pm 0.31	2.59 \pm 0.43	0.862

The table summarizes concentrations of total (labelled and unlabelled) metabolites in extracts of synaptosomes prepared from hippocampus obtained by HPLC. No significant differences were found in the concentrations of any metabolite measured. Results are presented as mean \pm SEM; $n=4-5$

significantly reduced when calculated for malate, citrate, glutamate and aspartate in hippocampal synaptosomes from synGLT-1 KO mice in comparison with controls ($p<0.001$, $n=4-5$; Fig. 7a).

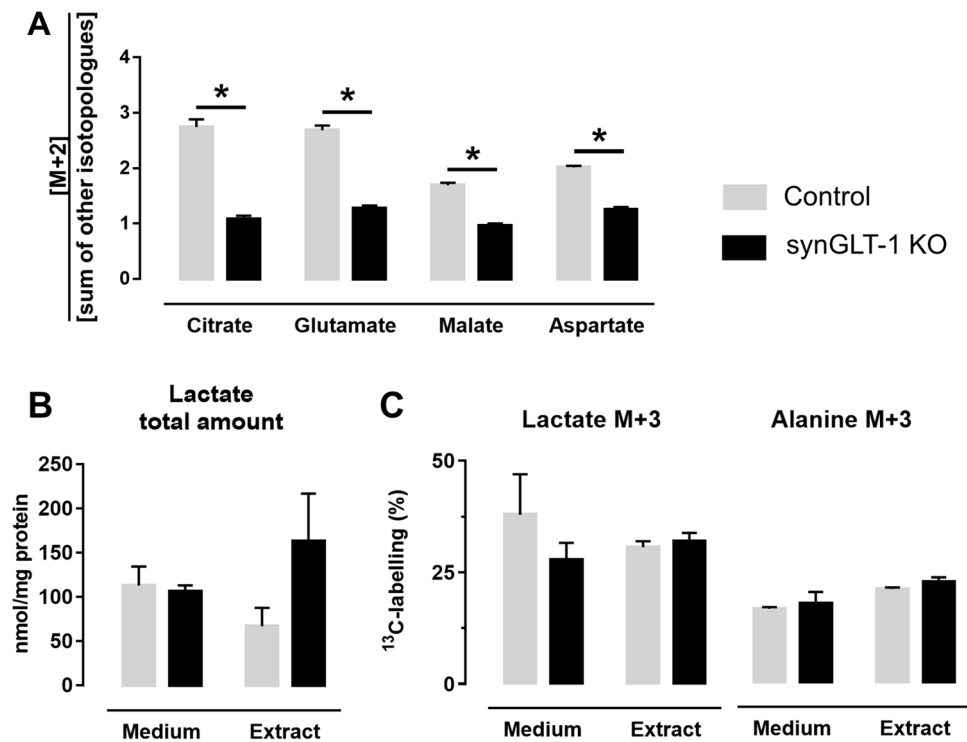


Fig. 7 Synaptic glutamate metabolism is reduced in the synGLT-1 KO hippocampus, whereas glycolysis is unaffected. Synaptosomes were purified from hippocampus of synGLT1 KO mice and littermate controls. Synaptic metabolism was assessed by incubating the synaptosomes 45 min with 2.5 mM [$U\text{-}^{13}\text{C}$]glucose in combination with 0.1 mM unlabelled glutamate. **a** Metabolism of [$U\text{-}^{13}\text{C}$]glucose gives rise to ^{13}C -labelling in TCA cycle intermediates and amino acids derived thereof, e.g. citrate, malate, glutamate and aspartate. Entry of unlabelled glutamate (taken up by neurons via GLT-1) will increase the unlabelled pool of TCA cycle intermediates. This entry of unlabelled glutamate was assessed as the ratio $[M+2]/[\text{sum of}$

other isotopologues] for the metabolites citrate, glutamate, malate and aspartate. **b, c** Metabolism of [$U\text{-}^{13}\text{C}$]glucose via glycolysis gives rise to [$U\text{-}^{13}\text{C}$]pyruvate (M+3), which can be metabolized to either [$1,2\text{-}^{13}\text{C}$]acetyl-CoA via pyruvate dehydrogenase, [$U\text{-}^{13}\text{C}$]alanine (M+3) via alanine aminotransferase or [$U\text{-}^{13}\text{C}$]lactate (M+3) via lactate dehydrogenase. Total lactate concentrations and percentage ^{13}C -labelling in lactate and alanine were determined in synaptosome extracts and the incubation medium using a lactate assay kit and GC-MS, respectively. Results are presented as mean \pm SEM; $n=4\text{--}5$; * $p<0.05$, Student's t -test

Glycolytic Activity

Breakdown of [$U\text{-}^{13}\text{C}$]glucose to [$U\text{-}^{13}\text{C}$]pyruvate via glycolysis and subsequent action of lactate dehydrogenase or alanine aminotransferase will lead to the formation of [$U\text{-}^{13}\text{C}$]lactate (M+3) and [$U\text{-}^{13}\text{C}$]alanine (M+3), respectively. Hence, the levels of lactate M+3 and alanine M+3 in synaptosomal preparations incubated with [$U\text{-}^{13}\text{C}$]glucose (in the presence of glutamate), as well as the total concentrations of these metabolites, are indicators of glycolytic activity. No significant differences between synGLT-1 KO and controls were detected for total concentrations or ^{13}C -enrichment of lactate and alanine in the media or extracts of hippocampal synaptosomes ($p>0.05$, $n=3\text{--}5$; Fig. 7b & c) following incubation in media containing 2.5 mM [$U\text{-}^{13}\text{C}$]glucose and 0.1 mM unlabelled glutamate.

Discussion

Here we present an extension of the first metabolic characterization study of the synGLT-1 KO mouse, conducted to assess whether functional implications for neuronal GLT-1 expression reported for the cerebral cortex also apply to other cerebral regions. We employed four experimental approaches using synGLT-1 KO and control mice, which collectively allows us to extend the statement that neuronal GLT-1 expression plays an important role in synaptic energy metabolism and aspartate homeostasis in the cerebral cortex, to also include the striatum and hippocampus. Moreover, our current study suggests that the nature of this role varies across brain regions.

Regional Similarities

The *ex vivo* evaluation of amino acid concentrations revealed similar reductions in aspartate levels and maintenance of glutamate levels in the hippocampus and striatum from synGLT-1 KO mice in comparison with controls, as previously reported for the cerebral cortex [28]. These data suggest a similar essential link between amino acid homeostasis and glutamate transport mediated by GLT-1 in neurons across these three distinct forebrain regions. Aspartate aminotransferase catalyses the conversion of α -ketoglutarate to glutamate at the expense of aspartate. The activity of aspartate aminotransferase is high in brain and is essential for maintenance of the vesicular glutamate pool [46]. It may be hypothesised that aspartate concentrations are reduced as a consequence of increased aspartate aminotransferase activity instated to sustain the synaptic glutamate pool in the absence of resupply by influx of glutamate mediated by GLT-1 expressed in axon terminals. Alternatively, glutamate provided to mitochondria specifically by GLT-1 expressed in neurons may be crucial for aspartate synthesis. This possibility is supported by the finding that *de novo* aspartate synthesis from glutamate occurs via the truncated TCA cycle [20].

Evaluation of [U - ^{13}C]glucose metabolism in hippocampal synaptosome preparations supports our interpretation of GLT-1 mediated glutamate uptake in neurons being crucial for mitochondrial glutamate metabolism (Fig. 7a). This is supported by a recent study assessing *ex vivo* metabolism in the hippocampus of a similar neuronal GLT-1 KO mouse model by administering [U - ^{13}C]glucose [7]. Interestingly, the direction and degree of change we observed in hippocampal preparations from synGLT-1 KO compared to controls is similar to that observed previously for the cerebral cortical preparations [28], suggesting a comparable dependence of synaptic mitochondrial glutamate metabolism on synaptic GLT-1-mediated glutamate uptake across the two regions. This may not be surprising, as the cerebral cortex and hippocampus have been shown to exhibit similar metabolic activity when measured *in vitro* [22] and *ex vivo* [47, 48]. However, other *ex vivo* and *in vivo* ^{13}C -mapping studies have detected a slower metabolism in the hippocampus compared to the cerebral cortex [49–51]. It should be kept in mind that *in vitro* preparations lack the activation from interbrain connectivity, which may affect regional metabolism differently and comparisons of brain regions from *in vitro* experiments should be made with care.

GLT-1 Expression at Axon Terminals Affects the Mitochondrial Density in the Hippocampus but not the Striatum

Mitochondria, the essential organelle for glutamate metabolism, are widely distributed in the cytoplasm of neurons and

astrocytes, including presynaptic axon terminals and within peri-synaptic astrocytic processes [52, 53]. Changes in mitochondrial distribution in neuronal processes are thought to be indicative of neuronal activity [54, 55]. In the hippocampus we discovered a remarkable increase in mitochondrial density within axon terminals as well as peri-synaptic astrocyte processes of synGLT-1 KO mice compared to control mice using EM. We recently reported increases of mitochondrial densities of similar magnitudes for the cerebral cortex of the synGLT-1 KO mice [28]. In the present study, however, we found no changes in these measures for the striatum. The lack of difference in the striatum could be because the presynaptic axon terminals in the striatum already carry high and perhaps maximum densities of mitochondria within controls, leaving little room for further increase in response to the loss of neuronal GLT-1 expression.

We observed significantly lower occurrences of tripartite synapses in dorsal striatum of both synGLT-1 KO and control, relative to the dorsal hippocampus (current study) and the cerebral cortex [28], reflecting another regional difference in the interdependence between neurons and astrocytes. This regional difference was paralleled by the lack of compensatory up-regulation of mitochondria in astrocytes within synGLT-1 KO striatum which was seen in synGLT-1 KO cerebral cortex [28] and hippocampus (current study), perhaps again reflecting the somewhat weaker interplay between neurons and astrocytes within striatum, compared to cerebral cortex and hippocampus.

In astrocytes, and possibly in neurons as well, one of the mechanisms determining the occurrence of mitochondria includes the physical and functional interactions between GLT-1 (Na^+ -dependent transporter) and the Na^+/Ca^{2+} exchanger NCX isoforms [56]. In short, NCX isoforms are enriched at peri-synaptic distal astrocyte processes and the Na^+ elevations arising with glutamate transport can reverse the mode (Na^+ out/ Ca^{2+} in) of NCX-mediated Ca^{2+} rises. This, in turn, can control the arrest and potentially accumulation of mitochondria in astrocyte processes [56]. Based on our results, we speculate that such activity-dependent regulation of mitochondria accumulation may be more robust for neurons and astrocytes in the cerebral cortex and hippocampus than in the striatum.

Presynaptic GLT-1 Expression in Hippocampus is Linked to Mitochondrial Efficiency but not Glycolytic Activity

Our functional metabolic studies of isolated hippocampal mitochondria obtained from the neuronal GLT-1 KO mice revealed a decreased mitochondrial oxygen consumption rate (OCR) in the presence of the ATP synthase inhibitor, oligomycin A. This suggests a reduced mitochondrial proton leak, i.e. reduced flow of protons across the inner

mitochondrial membrane independent of ATP turnover [57]. A lower mitochondrial proton leak indicates a tighter coupling between the proton motive force and ATP synthesis, and is thus indicative of enhanced mitochondrial efficiency in the synGLT-1 KO hippocampus. In contrast, no differences between OCR in the presence of oligomycin A were observed between mitochondria isolated from the cerebral cortex of synGLT-1 KO and control mice [28], signifying region-specific mitochondrial adaptations to neuronal GLT-1 KO. Hippocampal mitochondria have been shown to exhibit a larger basal proton leak and a larger potential for maximal uncoupled respiration in the presence of FCCP when compared to cerebral cortical mitochondria [26, 58], underlining that the different regional adaptations to neuronal GLT-1 KO could be dictated by inherent differences between these regions. The proton leak constitutes a large fraction of the resting mitochondrial membrane potential and is dependent on the mitochondrial membrane composition [59]. Since KO of neuronal GLT-1 has been shown to induce region specific changes in protein transcription [16], it could be that changes in mitochondrial membrane composition accounts for the lower proton leak in neuronal GLT-1 KO mice.

Interestingly, we have recently shown that isolated hippocampal mitochondria specifically exhibit a larger potential for maximal uncoupled respiration in the presence of FCCP when compared to cerebral cortical mitochondria, but only with pyruvate as respiratory substrate [26]. The maximal uncoupled OCR of the isolated hippocampal mitochondria from synGLT-1 KO mice was not significantly increased in the current study ($p = 0.089$) when compared to controls. However, it could be speculated that an overall enhanced maximal uncoupled respiration in the hippocampus compared to the cerebral cortex, could contribute to the mitochondrial adaptations observed in the synGLT-1 KO.

An improved mitochondrial function in the synGLT-1 KO brain is supported by our ultrastructural analysis pinpointing reduced inter-cristae distance in both the hippocampus, striatum (current study) and cerebral cortex [28], which has been shown to correlate with elevated ATP synthase activity [32]. This is in line with the significantly increased ATP synthesis in the cerebral cortex [28], which however, was not significantly altered in the hippocampus in the current study. The degree of synGLT-1-induced reduction of mitochondrial inter-cristae distance is greater for striatum (17%) than for hippocampus (10%). The degree of reduction of mitochondrial inter-cristae is even greater for the cerebral cortex (21.5%; [28]), pointing to additional regional differences in the mechanism of mitochondrial adaptation.

Whereas cerebral cortical synaptosomes from synGLT-1 KO mice exhibited reduced aspartate concentrations [28], hippocampal synaptosomes from neuronal GLT-1 KO showed unchanged aspartate levels following 45 min incubation with 2.5 mM [U- ^{13}C]glucose and 0.1 mM glutamate. It

cannot be ruled out that the decrease in total aspartate levels detected ex vivo for both regions may be reflected in the synaptic aspartate pool in vivo. Nevertheless, following an incubation of 45 min, the hippocampal synaptosome preparation from synGLT-1 KO mice appear to have overcome the neuronal GLT-1 KO-derived change in aspartate concentrations, whereas the cerebral cortical synaptosomes were unable to cope. In the presence of glutamate, hippocampal synaptosomes of neuronal GLT-1 KO mice showed no changes in the indicators of glycolytic activity (Fig. 7) in comparison with controls, demonstrating maintained glycolytic activity. This is in contrast to cerebral cortical synaptosomes of neuronal GLT-1 KO mice, in which the same indicators of glycolytic activity were elevated [28]. Altogether this suggests that the hippocampus and cerebral cortex display different dependencies on the provision of glutamate via GLT-1 in neurons for aspartate synthesis and/or diverse compensatory mechanisms, including modulation of glycolytic activity, are in place within these regions.

Astrocyte-Neuron Glutamine Transfer in the Striatum but not the Hippocampus is Coupled to Neuronal GLT-1

The ^{13}C -labelling derived from [1,2- ^{13}C]acetate reflects astrocytic metabolism [45]. In the current study, we observed a higher ^{13}C -labelling (%) in glutamate from [1,2- ^{13}C]acetate in striatum of synGLT-1 KO animals compared to control (Fig. 3d), which suggests an increased astrocytic TCA cycle metabolism and/or astrocyte-neuron glutamine transfer. Since glutamate is taken up via GLT-1 together with Na^+ , while K^+ is simultaneously expelled [60], continuation of glutamate uptake requires energy to maintain the Na^+/K^+ balance [61]. Considering that GLT-1 expression in neuronal terminals constitutes only 5–10% of the total expression of this transporter [4], it seems unlikely that abolishing expression of GLT-1 in neurons in itself would constitute an energy challenge for astrocytes, thus stimulating increased astrocytic uptake of glutamate ultimately leading to the observed increase in astrocytic TCA cycle metabolism in striatum of synGLT-1 KO animals. In dorsal striatum we observed maintained levels of mitochondrial densities in peri-synaptic astrocytes of synGLT-1 KO animals, which is in support of the synGLT-1 KO not constituting an energy challenge to the astrocytes requiring mitochondrial adaptations. Nevertheless, in the hippocampus (current study) and the cerebral cortex [28] a dramatic increase in mitochondrial occurrence in synaptic and non-synaptic astrocytic mitochondria was observed accompanied by unmodified astrocyte metabolism, suggesting that these other regions adapt differently than the dorsal striatum to the synGLT-1 KO.

Alternatively, the increased [4,5- ^{13}C]glutamate observed in the current study from [1,2- ^{13}C]acetate metabolism in

the striatum, could reflect an increased astrocyte-neuron transfer of [4,5-¹³C]glutamine induced by neuronal failure to take up and reuse glutamate locally at axon terminals and a compensatory increased reliance on the glutamate-glutamine cycle. Astrocyte TCA cycle metabolism is crucial for de novo synthesis of brain glutamate, and glutamine is a known astrocyte provided precursor for glutamate in neurons; hence, these results suggest a striatal involvement of neuronal GLT-1 in neurotransmitter glutamate homeostasis.

The observed increase in [4,5-¹³C]glutamate is not reflected in the labelling of glutamine. The latter amino acid is to a large extent released by the astrocytes and therefore, it is possible that an increase in glutamine labelling is present in the released pool of the amino acid and not the total glutamine pool, which was assayed in the current study. Alternatively, the unchanged glutamine labelling supports the interpretation that astrocyte TCA cycle metabolism may be unaffected by the synGLT-1 KO and the increased [4,5-¹³C]glutamate rather reflects an increase of astrocyte to neuron glutamine transfer. Taking into account that we show that despite genotype, dorsal striatum compared to hippocampus exhibited significantly lower occurrence of tripartite synapses, it is puzzling that striatum, but not hippocampus, exhibit indications of neuronal GLT-1 expression being linked to glutamine transfer.

Glutamate dependent excitotoxicity has been suggested to have a key contribution in the pathogenesis of Huntington's disease [62, 63]. One critical feature of Huntington's disease is the striatal vulnerability to neurodegeneration. This vulnerability may be associated with the large glutamatergic input from cortical afferents to the striatum, increasing its risk for excitotoxic injury. Interestingly, reduced expression of GLT-1 has been linked to Huntington's disease pathology [64, 65]. Moreover, deletion of neuronal GLT-1 has been found to produce a pattern of transcriptional dysregulation in the striatum similar to the one observed in Huntington's disease models [16], suggesting that specific impairments of neuronal glutamate uptake may be involved in disease development.

Conclusion

The glutamate transporter GLT-1 has been shown to be expressed in axon terminals in the hippocampus, cerebral cortex, and striatum [3–6]. Our results extend the functional relevance of neuronal GLT-1 expression previously established for cerebral cortex [28] to include two additional forebrain regions. In particular, we show that in the hippocampus and striatum the expression of the glutamate transporter GLT-1 in neurons is implicated in aspartate homeostasis, synaptic glutamate metabolism and mechanisms affecting mitochondrial distribution and ultrastructure in axon

terminals. Nevertheless, certain responses to the synGLT-1 KO were region specific, suggesting, for example, that in the hippocampus and cerebral cortex, but not in the striatum, mechanisms determining the mitochondrial density in axon terminals are sensitive to GLT-1 expression in neurons.

Acknowledgements This work was supported, in part, by a grant from Aase og Ejnar Danielsens Fond, and National Institute of Health grants NS066019, MH104318, MH105846, EY13079, and HD018655. NMR equipment used in this work was purchased via Grant #10–085264 from The Danish Research Council for Independent Research | Nature and Universe, 'Apotekerfonden af 1991', and the Danish Agency for Science, Technology and Innovation via the National Research Infrastructure funds. Laura F. McNair acknowledges the Department of Drug Design and Pharmacology (University of Copenhagen, Denmark) for granting of a PhD scholarship. Blanca Aldana is subsidized by a Grant from the Ministry of Science, Technology and Innovation (SECITI) of Mexico. Jens Andersen kindly thanks the Scholarship of Peter & Emma Thomsens for personal financial support. We thank Heidi Nielsen, Michaela C. Hohnholt, Nils Nyberg and Ursula Sonnewald for helpful assistance in the laboratory and data analysis.

Author Contribution LFM, PAR, CJA and HSW designed the experiments. LFM, JVA, JDN, YS, KDF, NWH, MD, CJA and BIA performed the experiments and data analysis. LFM and JVA wrote the manuscript with substantial input from PAR and BIA. PAR provided the mice from a colony maintained at Boston Children's Hospital. All authors have approved and provided critical input for the final manuscript.

Compliance with Ethical Standards

Conflict of interest The authors declare no conflict of interest.

Ethical Approval All applicable international, national, and/or institutional guidelines for the care and use of animals were followed. All animal experiments at Boston Children's Hospital were performed in accordance with National Institutes of Health guidelines, and were approved by the Boston Children's Hospital Institutional Animal Care and Use Committee. The experiments at the University of Copenhagen were approved by the Danish National Ethics Committee, and were performed according to the European Convention (ETS 123 of 1986).

References









1. Rimmele TS, Rosenberg PA (2016) GLT-1: The elusive presynaptic glutamate transporter. *Neurochem Int* 98:19–28
2. Danbolt NC, Furness DN, Zhou Y (2016) Neuronal vs glial glutamate uptake: Resolving the conundrum. *Neurochem Int* 98:29–45
3. Melone M, Belleli M, Conti F (2009) Synaptic localization of GLT-1a in the rat somatic sensory cortex. *Glia* 57:108–117
4. Furness DN, Dehnes Y, Akhtar AQ, Rossi DJ, Hamann M, Grutle NJ, Gundersen V, Holmseth S, Lehre KP, Ullensvang K, Wojewodzic M, Zhou Y, Attwell D, Danbolt NC (2008) A quantitative assessment of glutamate uptake into hippocampal synaptic terminals and astrocytes: new insights into a neuronal role for excitatory amino acid transporter 2 (EAAT2). *Neuroscience* 157:80–94
5. Chen W, Mahadomrongkul V, Berger UV, Bassan M, DeSilva T, Tanaka K, Irwin N, Aoki C, Rosenberg PA (2004) The glutamate transporter GLT1a is expressed in excitatory axon

- terminals of mature hippocampal neurons. *J Neurosci: Off J Soc Neurosci* 24:1136–1148
6. Petr GT, Schultheis LA, Hussey KC, Sun Y, Dubinsky JM, Aoki C, Rosenberg PA (2013) Decreased expression of GLT-1 in the R6/2 model of Huntington's disease does not worsen disease progression. *Eur J Neurosci* 38:2477–2490
 7. Zhou Y, Hassel B, Eid T, Danbolt NC (2019) Axon-terminals expressing EAAT2 (GLT-1; Slc1a2) are common in the fore-brain and not limited to the hippocampus. *Neurochem Int* 123:101–113
 8. Fischer KD, Houston ACW, Desai RI, Doyle MR, Bergman J, Mian M, Mannix R, Sulzer DL, Choi SJ, Mosharov EV, Hodgson NW, Bechtholt A, Miczek KA, Rosenberg PA (2018) Behavioral phenotyping and dopamine dynamics in mice with conditional deletion of the glutamate transporter GLT-1 in neurons: resistance to the acute locomotor effects of amphetamine. *Psychopharmacology* 235:1371–1387
 9. Ilieva H, Polymenidou M, Cleveland DW (2009) Non-cell autonomous toxicity in neurodegenerative disorders: ALS and beyond. *J Cell Biol* 187:761–772
 10. Sheldon AL, Robinson MB (2007) The role of glutamate transporters in neurodegenerative diseases and potential opportunities for intervention. *Neurochem Int* 51:333–355
 11. Dong X-x, Wang Y, Qin Z-h (2009) Molecular mechanisms of excitotoxicity and their relevance to pathogenesis of neurodegenerative diseases. *Acta Pharmacologica Sinica* 30:379
 12. Hynd MR, Scott HL, Dodd PR (2004) Glutamate-mediated excitotoxicity and neurodegeneration in Alzheimer's disease. *Neurochem Int* 45:583–595
 13. Kim K, Lee SG, Kegelman TP, Su ZZ, Das SK, Dash R, Dasgupta S, Barral PM, Hedvat M, Diaz P, Reed JC, Stebbins JL, Pellicchia M, Sarkar D, Fisher PB (2011) Role of excitatory amino acid transporter-2 (EAAT2) and glutamate in neurodegeneration: opportunities for developing novel therapeutics. *J Cell Physiol* 226:2484–2493
 14. Bates GP, Dorsey R, Gusella JF, Hayden MR, Kay C, Leavitt BR, Nance M, Ross CA, Scahill RI, Wetzel R, Wild EJ, Tabrizi SJ (2015) Huntington disease. *Nat Rev Dis Primers* 1:15005
 15. Masters CL, Bateman R, Blennow K, Rowe CC, Sperling RA, Cummings JL (2015) Alzheimer's disease. *Nat Rev Dis Primers* 1:15056
 16. Laprairie RB, Petr GT, Sun Y, Fischer KD, Denovan-Wright EM, Rosenberg PA (2019) Huntington's disease pattern of transcriptional dysregulation in the absence of mutant huntingtin is produced by knockout of neuronal GLT-1. *Neurochem Int* 123:85–94
 17. McKenna MC (2013) Glutamate pays its own way in astrocytes. *Front Endocrinol* 4:191
 18. McKenna MC, Stridh MH, McNair LF, Sonnewald U, Waagepetersen HS, Schousboe A (2016) Glutamate oxidation in astrocytes: roles of glutamate dehydrogenase and aminotransferases. *J Neurosci Res* 94:1561–1571
 19. Hohnholt MC, Andersen VH, Andersen JV, Christensen SK, Karaca M, Maechler P, Waagepetersen HS (2018) Glutamate dehydrogenase is essential to sustain neuronal oxidative energy metabolism during stimulation. *J Cereb Blood Flow Metab: Off J Int Soc Cereb Blood Flow Metab* 38:1754–1768
 20. Nissen JD, Pajacka K, Stridh MH, Skyyt DM, Waagepetersen HS (2015) Dysfunctional TCA-cycle metabolism in glutamate dehydrogenase deficient astrocytes. *Glia* 63:2313–2326
 21. Olstad E, Qu H, Sonnewald U (2007) Glutamate is preferred over glutamine for intermediary metabolism in cultured cerebellar neurons. *J Cereb Blood Flow Metab: Off J Int Soc Cereb Blood Flow Metab* 27:811–820
 22. McNair LF, Kornfelt R, Walls AB, Andersen JV, Aldana BI, Nissen JD, Schousboe A, Waagepetersen HS (2017) Metabolic characterization of acutely isolated hippocampal and cerebral cortical slices using [U-13C]glucose and [1,2-13C]acetate as substrates. *Neurochem Res* 42:810–826
 23. Kleinridders A, Ferris HA, Reyzer ML, Rath M, Soto M, Manier ML, Spraggins J, Yang Z, Stanton RC, Caprioli RM, Kahn CR (2018) Regional differences in brain glucose metabolism determined by imaging mass spectrometry. *Mol Metab* 12:113–121
 24. Aoki C, Milner TA, Berger SB, Sheu KF, Blass JP, Pickel VM (1987) Glial glutamate dehydrogenase: ultrastructural localization and regional distribution in relation to the mitochondrial enzyme, cytochrome oxidase. *J Neurosci Res* 18:305–318
 25. Aoki C, Milner TA, Sheu KF, Blass JP, Pickel VM (1987) Regional distribution of astrocytes with intense immunoreactivity for glutamate dehydrogenase in rat brain: implications for neuron-glia interactions in glutamate transmission. *J Neurosci: Off J Soc Neurosci* 7:2214–2231
 26. Andersen JV, Jakobsen E, Waagepetersen HS, Aldana BI (2019) Distinct differences in rates of oxygen consumption and ATP synthesis of regionally isolated non-synaptic mouse brain mitochondria. *J Neurosci Res* 97:961–974
 27. Petersen MH, Willert CW, Andersen JV, Waagepetersen HS, Skotte NH, Norremolle A (2019) Functional differences between Synaptic Mitochondria from the Striatum and the Cerebral Cortex. *Neuroscience* 406:432–443
 28. McNair LF, Andersen JV, Aldana BI, Hohnholt MC, Nissen JD, Sun Y, Fischer KD, Sonnewald U, Nyberg N, Webster SC, Kapur K, Rimmele TS, Barone I, Hawks-Mayer H, Lipton JO, Hodgson NW, Hensch TK, Aoki CJ, Rosenberg PA, Waagepetersen HS (2019) Deletion of neuronal GLT-1 in mice reveals its role in synaptic glutamate homeostasis and mitochondrial function. *J Neurosci: Off J Soc Neurosci* 39:4847–4863
 29. Petr GT, Sun Y, Frederick NM, Zhou Y, Dhamne SC, Hameed MQ, Miranda C, Bedoya EA, Fischer KD, Armsen W, Wang J, Danbolt NC, Rotenberg A, Aoki CJ, Rosenberg PA (2015) Conditional deletion of the glutamate transporter GLT-1 reveals that astrocytic GLT-1 protects against fatal epilepsy while neuronal GLT-1 contributes significantly to glutamate uptake into synaptosomes. *J Neurosci: Off J Soc Neurosci* 35:5187–5201
 30. Andersen JV, Christensen SK, Nissen JD, Waagepetersen HS (2017) Improved cerebral energetics and ketone body metabolism in db/db mice. *J Cereb Blood Flow Metab: Off J Int Soc Cereb Blood Flow Metab* 37:1137–1147
 31. Andersen JV, Christensen SK, Aldana BI, Nissen JD, Tanila H, Waagepetersen HS (2017) Alterations in cerebral cortical glucose and glutamine metabolism precedes amyloid plaques in the APP^{swe}/PSEN1^{ΔE9} mouse model of Alzheimer's disease. *Neurochem Res* 42:1589–1598
 32. Gomes LC, Di Benedetto G, Scorrano L (2011) Essential amino acids and glutamine regulate induction of mitochondrial elongation during autophagy. *Cell Cycle (Georgetown, Tex)* 10:2635–2639
 33. Benjamini Y, Hochberg Y (1995) Controlling the false discovery rate: a practical and powerful approach to multiple testing. *J Royal Stat Soc: B* 57:289–300
 34. Lee JY, Ristow M, Lin X, White MF, Magnuson MA, Hennighausen L (2006) RIP-Cre revisited, evidence for impairments of pancreatic beta-cell function. *J Biol Chem* 281:2649–2653
 35. Schmidt-Supprian M, Rajewsky K (2007) Vagaries of conditional gene targeting. *Nat Immunol* 8:665–668
 36. Harno E, Cottrell EC, White A (2013) Metabolic pitfalls of CNS Cre-based technology. *Cell Metab* 18:21–28
 37. Hu H, Cavendish JZ, Agmon A (2013) Not all that glitters is gold: off-target recombination in the somatostatin-IRES-Cre

- mouse line labels a subset of fast-spiking interneurons. *Front Neural Circuits* 7:195
38. Stuber GD, Stamatakis AM, Kantak PA (2015) Considerations when using cre-driver rodent lines for studying ventral tegmental area circuitry. *Neuron* 85:439–445
 39. Moffett JR, Ross B, Arun P, Madhavarao CN, Nambodiri AM (2007) N-Acetylaspartate in the CNS: from neurodiagnostics to neurobiology. *Prog Neurobiol* 81:89–131
 40. Baslow MH (2010) A novel key-lock mechanism for inactivating amino acid neurotransmitters during transit across extracellular space. *Amino Acids* 38:51–55
 41. Hassel B, Sonnewald U, Fonnun F (1995) Glial-neuronal interactions as studied by cerebral metabolism of [2-13C]acetate and [1-13C]glucose: an ex vivo 13C NMR spectroscopic study. *J Neurochem* 64:2773–2782
 42. Qu H, Haberg A, Haraldseth O, Unsgard G, Sonnewald U (2000) (13)C MR spectroscopy study of lactate as substrate for rat brain. *Dev Neurosci* 22:429–436
 43. Lundgaard I, Li B, Xie L, Kang H, Sanggaard S, Haswell JD, Sun W, Goldman S, Blekot S, Nielsen M, Takano T, Deane R, Nedergaard M (2015) Direct neuronal glucose uptake heralds activity-dependent increases in cerebral metabolism. *Nat Comm* 6:6807
 44. Haberg A, Qu H, Haraldseth O, Unsgard G, Sonnewald U (1998) In vivo injection of [1-13C]glucose and [1,2-13C]acetate combined with ex vivo 13C nuclear magnetic resonance spectroscopy: a novel approach to the study of middle cerebral artery occlusion in the rat. *J Cereb Blood Flow Metab: Off J Int Soc Cereb Blood Flow Metab* 18:1223–1232
 45. Sonnewald U, Westergaard N, Schousboe A, Svendsen JS, Unsgard G, Petersen SB (1993) Direct demonstration by [13C] NMR spectroscopy that glutamine from astrocytes is a precursor for GABA synthesis in neurons. *Neurochem Int* 22:19–29
 46. Palaiologos G, Hertz L, Schousboe A (1989) Role of aspartate aminotransferase and mitochondrial dicarboxylate transport for release of endogenously and exogenously supplied neurotransmitter in glutamatergic neurons. *Neurochem Res* 14:359–366
 47. Wang J, Jiang L, Jiang Y, Ma X, Chowdhury GM, Mason GF (2010) Regional metabolite levels and turnover in the awake rat brain under the influence of nicotine. *J Neurochem* 113:1447–1458
 48. Tiwari V, Patel AB (2014) Pyruvate carboxylase and pentose phosphate fluxes are reduced in AbetaPP-PS1 mouse model of Alzheimer's disease: a (1)(3)C NMR study. *J Alzheimer's Dis* 41:387–399
 49. Sokoloff L, Reivich M, Kennedy C, Des Rosiers MH, Patlak CS, Pettigrew KD, Sakurada O, Shinohara M (1977) The [14C]deoxyglucose method for the measurement of local cerebral glucose utilization: theory, procedure, and normal values in the conscious and anesthetized albino rat. *J Neurochem* 28:897–916
 50. Hyder F, Fulbright RK, Shulman RG, Rothman DL (2013) Glutamatergic function in the resting awake human brain is supported by uniformly high oxidative energy. *J Cereb Blood Flow Metab: Off J Int Soc Cereb Blood Flow Metab* 33:339–347
 51. de Graaf RA, Mason GF, Patel AB, Rothman DL, Behar KL (2004) Regional glucose metabolism and glutamatergic neurotransmission in rat brain in vivo. *Proc Nat Acad Sci USA* 101:12700–12705
 52. Peters A, Palay SL, Webster HD (1978) The fine structure of the nervous system: the neurons and supporting cells, by Alan Peters, Sanford L. Palay, and Henry Def. Webster, 395 pp, illustrated, W. B. Saunders Company, Philadelphia, 1976. *Ann Neurol* 4:588–588
 53. Jackson JG, Robinson MB (2018) Regulation of mitochondrial dynamics in astrocytes: Mechanisms, consequences, and unknowns. *Glia* 66:1213–1234
 54. Schwarz TL (2013) Mitochondrial trafficking in neurons. *Cold Spring Harbor perspectives in biology* 5
 55. Misgeld T, Schwarz TL (2017) Mitostasis in neurons: maintaining mitochondria in an extended cellular architecture. *Neuron* 96:651–666
 56. Robinson MB, Jackson JG (2016) Astroglial glutamate transporters coordinate excitatory signaling and brain energetics. *Neurochem Int* 98:56–71
 57. Brand MD, Nicholls DG (2011) Assessing mitochondrial dysfunction in cells. *Biochem J* 435:297–312
 58. Sauerbeck A, Pandya J, Singh I, Bittman K, Readnow R, Bing G, Sullivan P (2011) Analysis of regional brain mitochondrial bioenergetics and susceptibility to mitochondrial inhibition utilizing a microplate based system. *J Neurosci Methods* 198:36–43
 59. Jastroch M, Divakaruni AS, Mookerjee S, Treberg JR, Brand MD (2010) Mitochondrial proton and electron leaks. *Essays Biochem* 47:53–67
 60. Danbolt NC (2001) Glutamate uptake. *Progr Neurobiol* 65:1–105
 61. Attwell D, Laughlin SB (2001) An energy budget for signaling in the grey matter of the brain. *J Cereb Blood Flow Metab: Off J Int Soc Cereb Blood Flow Metab* 21:1133–1145
 62. Beal MF, Ferrante RJ, Swartz KJ, Kowall NW (1991) Chronic quinolinic acid lesions in rats closely resemble Huntington's disease. *J Neurosci: Off J Soc Neurosci* 11:1649–1659
 63. Estrada Sanchez AM, Mejia-Toiber J, Massieu L (2008) Excitotoxic neuronal death and the pathogenesis of Huntington's disease. *Arch Med Res* 39:265–276
 64. Behrens PF, Franz P, Woodman B, Lindenberg KS, Landwehrmeyer GB (2002) Impaired glutamate transport and glutamate-glutamine cycling: downstream effects of the Huntington mutation. *Brain: J Neurol* 125:1908–1922
 65. Skotte NH, Andersen JV, Santos A, Aldana BI, Willert CW, Norremolle A, Waagepetersen HS, Nielsen ML (2018) Integrative characterization of the R6/2 mouse model of Huntington's disease reveals dysfunctional astrocyte metabolism. *Cell Rep* 23:2211–2224

Publisher's Note Springer Nature remains neutral with regard to jurisdictional claims in published maps and institutional affiliations.

Affiliations

Laura F. McNair¹  · Jens V. Andersen¹  · Jakob D. Nissen¹  · Yan Sun² · Kathryn D. Fischer² · Nathaniel W. Hodgson²  · Muzi Du³ · Chiye J. Aoki^{3,4}  · Helle S. Waagepetersen¹  · Paul A. Rosenberg^{2,5}  · Blanca I. Aldana¹ 

¹ Department of Drug Design and Pharmacology, University of Copenhagen, 2 Universitetsparken, Copenhagen 2100, Denmark

² Department of Neurology and the F.M. Kirby Neurobiology Center, Boston Children's Hospital, Boston, MA 02115, USA

³ Center for Neural Science, New York University, New York, NY 10003, USA

⁴ Neuroscience Institute, New York University Langone Medical Center, New York, NY 10016, USA

⁵ Program in Neuroscience, Harvard Medical School, Boston, MA 02115, USA